

## Environmental effects on measured structural frequencies— model prediction of short-term shift during heavy rainfall and comparison with full-scale observations

Maria I. Todorovska<sup>\*,†,‡</sup> and Yousef Al Rjoub<sup>§</sup>

*Civil and Environmental Engineering Department, University of Southern California, Los Angeles, CA 90089-2531, U.S.A.*

### SUMMARY

The sensitivity of measurements of the frequencies of vibration of structures to environmental factors, such as weather, has been of interest for structural identification and health monitoring, as changes in these frequencies are often used as indicators of degradation of the structure. This paper presents a simple 2D soil–structure interaction model that can predict shifts in the apparent frequency of a building due to water saturation of the soil during heavy rainfall, and recovery as the degree of saturation decreases. The soil is modeled as a porous half-space, dry or fully saturated with *viscous* fluid (water in this case), the motion of which is described by Biot's theory of wave propagation in fluid-saturated porous media. This model is a generalization of a previous model considered by the authors to more realistic soils—with finite permeability and saturated with viscous fluids. Results of model predictions are shown for model parameters that correspond approximately to the NS response of Millikan library in Pasadena, CA, and are compared with the observed trends at the same site under ambient noise excitation (up to about 3.5% increase in the first frequency during heavy rainfall, and recovery within about a week following the rainfall). Results are shown for a range of values of soil permeability as well as for undrained soil (elastic solid with Poisson ratio close to 0.5). The model predictions agree qualitatively with the observed effects at Millikan library, but the analysis does not exclude other possible causes for the observed effect. Copyright © 2008 John Wiley & Sons, Ltd.

**KEY WORDS:** structural health monitoring; structural frequency; environmental effects; soil–structure interaction; poroelasticity; Biot theory

### INTRODUCTION

In structural health monitoring research, variations of the observed frequencies of buildings are often used to make inferences about the change of the state of health of their structure. To this

---

\*Correspondence to: M. I. Todorovska, Civil and Environmental Engineering Department, University of Southern California, Los Angeles, CA 90089-2531, U.S.A.

†E-mail: mtodorov@usc.edu

‡Research Professor.

§Formerly graduate student.

*Received 27 June 2007  
Revised 7 January 2008  
Accepted 26 February 2008*

end, numerous methods have been proposed in the literature on how to trace these changes in time. In such studies it is usually overlooked that the frequency measured is that of the soil–structure system, which changes also due to changes in the soil. The fixed-base frequency, which is the one affected directly by loss of stiffness caused by damage, is rarely available as it requires more extensive instrumentation than that available in most instrumented buildings. It has been recognized that the measured frequencies are sensitive to the amplitudes of response, to environmental factors (such as weather, including temperature, strong winds, even rainfall), and also to changes in the boundary conditions (e.g. at the contact with the soil), which is referred to as ‘noise’ of the structural health monitoring methods [1,2]. Efforts to quantify the effects of weather include full-scale observations, such as those at Millikan library in Pasadena, CA [3], and field observations on scaled models, such as those at the NEES filed testing site in Garner Valley, CA [4]. This work attempts to explain the observed effects at Millikan library, described in the following.

#### *Observations at Millikan library*

Millikan library is a 9-story reinforced concrete (RC) structure, with plan dimensions  $21 \times 23$  m, and vertically extending 43.9 m above grade and 48.2 m above basement level. Resistance to lateral forces is provided by a moment resisting frame, stiff RC shear walls on the east and west sides of the building, providing resistance to lateral forces mainly in the NS direction, and a RC central core, providing resistance to lateral forces mainly in the EW direction. The foundation system is composed of a central pad 9.75 m wide by 1.2 m deep, which extends across the building to the shear walls on the east and west sides. The local soil can be characterized as alluvium, with average shear wave velocity in the top 30 m of about 300 m/s, and depth to ‘bedrock’ of about 275 m. The alluvium consists of medium to dense sands mixed with gravels, and the water table appears to be at about 11 m in depth [3,5].

Millikan library has a long history of monitoring (since 1967) using ambient noise, forced vibrations, and earthquake excitation. Permanent and temporary changes in its frequencies have been studied, and most recently summarized in Clinton *et al.* [3]. The permanent change has been decrease with time, from 1.45 to 1.19 Hz for EW vibrations, and from 1.9 to 1.72 Hz for NS vibrations, both evident during small amplitude vibrations. The lowest measured values occurred during the strongest shaking, and were first observed during the 1971 San Fernando earthquake [6]. During the 1994 Northridge earthquake, the low values were 0.94 Hz for EW vibrations, and 1.33 Hz for NS vibrations.

Since February 2001, continuous data streams of the 9th floor response have been recorded by a tri-axial 24-bit accelerometer, which is one of the stations of the California Integrated Seismic Network. This has enabled monitoring of changes in the building’s apparent frequencies on different time scales [3]. Further, weather data from the nearby JPL Weather station, located about 8.5 km north of the building, has been available for a period of about 2.5 years following the installation of this sensor. This has enabled one to explore possible correlations of the changes in building frequency with weather (i.e. temperature, wind, and rain). The observed correlation with rainfall is *increase* in the first and second apparent EW and NS frequencies, and in the first torsional frequency during *heavy* rainfall (greater than 40 mm per day) in a matter of hours, and recovery in about a week following the rain [3]. For example, in early February of 2003, when over 100 mm rain fell over a period of 2 days, an increase in about 3% was measured for the EW and the torsional frequencies, followed by a slow decay over a period of about 10

days (see Figure 9 in [3]). The measured change in the NS frequency was smaller (slightly less than 1%). Clinton *et al.* [3] noted that this increase in frequencies occurred in spite of the fact that strong winds that often accompany heavy rainfall tend to decrease the system frequencies by exciting larger amplitudes of response (by up to 3% in dry weather). Further, they noted an increase in the system frequencies with temperature (about 1–2% on very hot days with the temperature near 40°C). For wind and temperature, the recovery is practically instantaneous, whereas for rainfall it is slow, and can take about a week. Further, they noted an observed increase by 4% of EW frequency due to added partitions to convert three of the stories to office space, whereas the reduction mass due to removal of the books did not cause much change.

#### *Hypothesis and objectives of this work*

For buildings on flexible soil, the energy of the response is concentrated around the frequencies of the soil–structure system, which are different from the building fixed-base frequencies. Let  $f_{\text{sys}}$  be the lowest such frequency (a result of coupling with the fundamental fixed-base frequency  $f_1$ ). Then  $f_{\text{sys}}$  and  $f_1$  are related by

$$f_{\text{sys}}^{-2} = f_1^{-2} + f_{\text{H}}^{-2} + f_{\text{R}}^{-2} \quad (1)$$

where  $f_{\text{H}}$  and  $f_{\text{R}}$  represent the horizontal and rocking frequencies of a rigid building on flexible soil. Equation (1) implies that always  $f_1 > f_{\text{sys}}$ , and that  $f_{\text{sys}}$  changes whenever there is a change in the stiffness of the soil, or a change in the contact between the foundation and the soil, via change in  $f_{\text{H}}$  and  $f_{\text{R}}$ . Hence,  $f_{\text{sys}}$  would change due to changes in the soil resulting from water saturation following heavy rainfall, and would recover gradually to its original value (preceding the heavy rainfall) as the soil dries out.

The objective of this paper is to find out the trend and order of magnitude of such changes using a simple soil–structure interaction model of a building on a rigid embedded foundation in a half-space. The effect of the water saturation is accounted for by modeling the soil as a poroelastic medium [7], which is dry before the heavy rainfall, and fully saturated during the heavy rainfall. A similar model as the one in this paper was considered recently by the same authors [8,9], which predicted a shift in frequency that agreed qualitatively with the observations at Millikan library. The earlier model considered only ideal (inviscid) fluids, hence, neglecting the effects of the seepage force in the soil. The model in this paper is a generalization of the model in Todorovska and Al Rjoub [8,9] to viscous pore fluids and soils with finite permeability.

The effects of soil–structure interaction on the response of Millikan library have been studied in detail [5,10]. Experiments have shown that, for NS vibrations the base moves as a rigid body [10], and as much as 30% of the roof response is due to rigid body rocking [11], whereas for EW vibrations it behaves as one on a flexible foundation with a stiff central core [10]. Hence, the soil–structure interaction effects are significant for this building, and a rigid foundation model might be appropriate for its NS response [5]. Soil–structure interaction for rigid foundations in poroelastic soils has been considered by a number of authors since the 1980s (e.g. [12–15]). A detailed recent review of such work can be found in [8].

The next section presents the theoretical model, which is followed by a presentation of numerical results for model parameters that correspond approximately to the NS response of Millikan library, for which a rigid foundation model may be appropriate. Results are shown for the foundation complex stiffness matrix and for the system response to horizontal driving force. Results are shown for a range of values of the permeability of the skeleton, as well as for undrained

soil, modeled as a solid with a large Poisson ratio (close to 0.5). Finally, the predicted shifts by the model are compared with the observation at Millikan library, and conclusions are drawn.

### MODEL

The simple two-dimensional soil–structure interaction model for in-plane motions is shown in Figure 1. The building is represented as a shear beam supported by a circular rigid foundation embedded in a homogeneous and isotropic *poroelastic* half-space. The center of curvature of the foundation is at some point  $O_1$  along the  $z$ -axis, in general above point  $O$  (see Figure 2). The shear beam has height  $H$ , width  $W$ , and mass per unit length  $m_b$  (in the  $y$ -direction, perpendicular to the cross-section showed in Figure 1). The foundation has width  $2a$ , depth  $h$ , and mass per unit length  $m_{\text{fnd}}$ . The response of the foundation is described by the horizontal and vertical displacements of point  $O$ ,  $\Delta$  and  $V$ , and the rotation angle  $\varphi$  (positive clockwise). The building moves as a rigid body, with translations  $\Delta$  and  $V$ , and rotation  $\varphi$ , and also deflects due to elastic deformation (Figure 1). The horizontal displacement at the top of the building due to its elastic deformation is  $u_b^{\text{rel}}$ . The shear wave velocity in the building is  $V_{S,b}$ , which implies first mode fixed-base frequency  $f_1 = V_{S,b}/(4H)$  [16]. The damping in the building is neglected. The excitation is a plane P or SV wave, with incident angle  $\theta_0$ , or a (surface) Rayleigh wave.

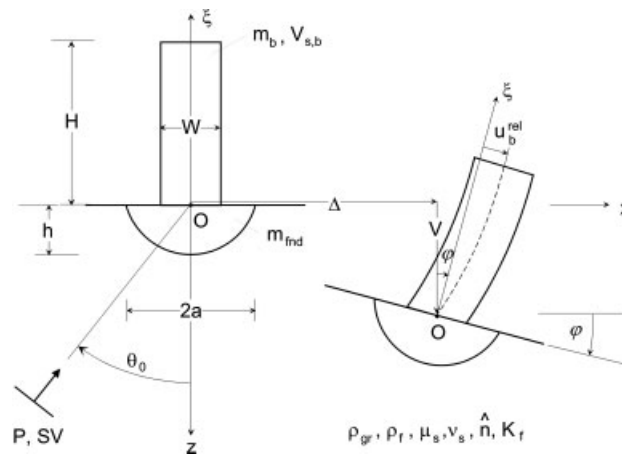


Figure 1. The model.

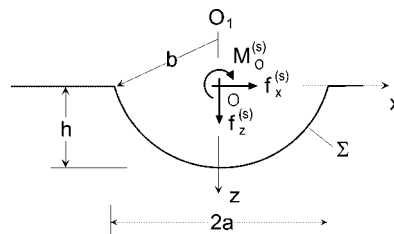


Figure 2. The excavation and forces acting on the soil.

The motion in the half-space is described by the linearized theory of wave propagation in fluid-saturated poroelastic media formulated by Biot [7]. The two-phase medium is composed of a solid skeleton, formed by the grains, and fluid occupying completely all voids. The properties of this mixture are defined by the shear modulus and Poisson's ratio of the skeleton  $\mu_s$  and  $\nu_s$ , the bulk modulus of the fluid  $K_f$ , the porosity  $\hat{n}$ , the mass density of the grains  $\rho_{gr}$  comprising the skeleton, and the density of the fluid  $\rho_f$ , defined per unit volume of pure material. This implies shear wave velocity of the dry mixture  $V_{s,dry} = \sqrt{\mu_s / [(1 - \hat{n})\rho_{gr}]}$ . The skeleton and the foundation are perfectly bonded to each other. The motion of the fluid along the contact surface relative to that of the solid is constrained by the drainage condition. It is assumed in this article that the foundation can be either completely permeable, allowing for free drainage of the pore fluid, or completely impermeable. These conditions would affect the foundation complex stiffness matrix, and the foundation driving forces. The half-space surface can also be either perfectly sealed or unsealed, and this would affect the free-field motion [17]. A soil-structure interaction model of similar geometry but in elastic half-space has been considered earlier for incident SH waves [18,19], and for incident P, SV, and Rayleigh waves [16,20].

A closed-form solution is obtained by (1) expanding the scattered waves (a perturbation to the free-field motion caused by the presence of the foundation) in a series of outgoing cylindrical waves (represented by Hankel functions in space), (2) expressing the coefficients of this expansion in terms of the (known) coefficients of expansion of the free-field motion and the (unknown) motion of the rigid foundation through the continuity of displacements at the contact surface, and (3) solving for the motion of the foundation from the dynamic equilibrium of the foundation. In this process, the zero-stress condition on the half-space surface, which is automatically satisfied by the free-field motion, is relaxed for the scattered waves, as in [8], in which case, the entries of the complex stiffness matrix for a semi-circular foundation (as considered in this article) are half of those for a cylinder in a full space.

#### *Wave propagation in fluid-saturated poroelastic medium*

The motion in the soil is assumed to be governed by Biot's theory of wave propagation in a fully saturated poroelastic medium [7], which was postulated based on the assumption that the motion of the solid matrix is wave motion, whereas that of the fluid relative to the solid is a diffusion process described by Darcy's law. Further, this theory is based on the assumptions that (i) the flow of the fluid in the pores is laminar (Reynolds number is less than 2000), which imposes an upper bound on the frequency for which the theory is valid; (ii) the size of the unit element of the solid-fluid mixture is much smaller than the wavelength of the motions considered, and (iii) the size of the unit element of the mixture is large compared with the size of the pores. Then the motion of the solid and that of the fluid is described by the following two coupled equations of motion

$$\begin{aligned} \mu \nabla^2 \tilde{\mathbf{u}} + \text{grad}[(\lambda + \mu)e + Q\epsilon] &= \frac{\partial^2}{\partial t^2} (\rho_{11}\mathbf{u} + \rho_{12}\mathbf{U}) + \hat{b} \frac{\partial}{\partial t} (\mathbf{u} - \mathbf{U}) \\ \text{grad}[Qe + R\epsilon] &= \frac{\partial^2}{\partial t^2} (\rho_{11}\mathbf{u} + \rho_{12}\mathbf{U}) - \hat{b} \frac{\partial}{\partial t} (\mathbf{u} - \mathbf{U}) \end{aligned} \quad (2)$$

where  $\mathbf{u}$  and  $\mathbf{U}$  are displacement vectors describing the motion of the skeleton and of the pore fluid,  $\rho_{11}, \rho_{12}, \rho_{22}$  are dynamic mass coefficients,  $\hat{b}$  is a coefficient of dissipation,  $\lambda, \mu, Q, R$  are

material constants of the mixture, and

$$\begin{aligned} e &= \text{div}(\mathbf{u}) \\ \epsilon &= \text{div}(\mathbf{U}) \end{aligned} \quad (3)$$

The coefficient of dissipation  $\hat{b}$  depends on the skeleton permeability and fluid viscosity as

$$\hat{b} = \hat{n}^2 \frac{\hat{\mu}}{\hat{k}} \quad (4)$$

where  $\hat{n}$  is the porosity,  $\hat{\mu}$  is the absolute viscosity of the fluid in units  $\text{Pa s} = \text{kg}/(\text{m s})$ , and  $\hat{k}$  is the skeleton intrinsic permeability, which depends only on the properties of the skeleton, in units  $\text{m}^2$ . Hence,  $\hat{b}/\omega$  has units of mass density, and can be used to estimate the significance of the effect of the seepage force. When  $\hat{b}/\omega$  is much smaller than the dynamic mass coefficients  $\rho_{11}, \rho_{12}, \rho_{22}$ , the seepage force is much smaller than the inertia forces and its effects are negligible. This happens when the fluid viscosity is small, or the permeability of the skeleton is large, and, for fixed viscosity and permeability, when the frequency of motion is high enough.

The constitutive relationships for the unit cube of the mixture are

$$\begin{aligned} \tau_{ij} &= (\lambda e + Q\epsilon)\delta_{ij} + 2\mu\epsilon_{ij} \\ s &= Qe + R\epsilon \\ \sigma_{ij}^{\text{tot}} &= \tau_{ij} + s\delta_{ij} \end{aligned} \quad (5)$$

where  $\tau_{ij}$  is the stress tensor acting on the skeleton,  $s$  is the normal stress acting on the fluid,  $\sigma_{ij}^{\text{tot}}$  is the total stress tensor (all per unit area of the mixture),  $\epsilon_{ij}$  is the strain tensor for the skeleton, and  $\delta_{ij}$  is the Kronecker delta. The normal stress  $s$  is related to the pore pressure  $p$  (positive when in compression, and per unit area of the fluid inside the pores) by

$$s = -p\hat{n} \quad (6)$$

Helmholtz decomposition of each of the displacement vectors

$$\begin{aligned} \mathbf{u} &= \text{grad}\phi + \text{curl}\psi \\ \mathbf{U} &= \text{grad}\Phi + \text{curl}\Psi \end{aligned} \quad (7)$$

where  $\phi$  and  $\psi$  are potentials for the solid, and  $\Phi$  and  $\Psi$  of the pore fluid, leads to the decoupling of system of Equations (2) into separate equations, one involving only the scalar potentials  $\phi$  and  $\Phi$ , and another involving only the vector potentials  $\psi$  and  $\Psi$ . Further, for harmonic excitation, the potentials can be represented as

$$\begin{aligned} \phi &= c_1 \exp[kx - \omega t] \\ \Phi &= c_2 \exp[kx - \omega t] \end{aligned} \quad (8)$$

and

$$\begin{aligned} \psi &= \mathbf{c}_3 \exp[kx - \omega t] \\ \Psi &= \mathbf{c}_4 \exp[kx - \omega t] \end{aligned} \quad (9)$$

Substitution of (8) and (9) in the decoupled equations of motion results in four separate wave equations for  $\phi$ ,  $\Phi$ ,  $\psi$ , and  $\Psi$ , such that the potentials for the fluid up to scaling factors are identical to those of the solid. The equations for the scalar potentials have two distinct solutions,

characterized by velocities of propagation

$$V_{Pj} = \sqrt{\frac{2A}{B \mp (B^2 - 4AC)^{1/2}}}, \quad j = 1, 2 \quad (10a)$$

whereas the solution for the vector potential has only one solution, characterized by the velocity of propagation

$$V_S = \sqrt{\frac{\mu(\rho_{22} + i\hat{b}/\omega)}{\rho_{11}\rho_{22} - \rho_{12}^2 + (\rho_{11} + \rho_{22} + 2\rho_{12})i\hat{b}/\omega}} \quad (10b)$$

where

$$A = PR - Q^2 \quad (10c)$$

$$B = \rho_{11}R + \rho_{22}P - 2\rho_{12}Q + \frac{i\hat{b}}{\omega}(P + R + 2Q) \quad (10d)$$

$$C = \rho_{11}\rho_{22} - \rho_{12}^2 + \frac{i\hat{b}}{\omega}(\rho_{11} + \rho_{22} + 2\rho_{12}) \quad (10e)$$

$$P = \lambda + 2\mu \quad (10f)$$

This means that two different P-waves, and one S-wave exist in fluid-saturated porous media. The two P-waves differ significantly in their velocity of propagation and the degree of attenuation with distance, and are referred to as 'fast' and 'slow' P-wave. The fast P-wave and the S-wave behave much like the P- and S-waves in an elastic medium, and are attenuated little with distance (due to the seepage force). The slow P-wave is characterized by much higher attenuation, and hence exists only locally, where it has been generated. This fact may explain why the slow P-wave was first observed only in 1980 [21], about quarter of a century after being predicted by Biot's theory [7].

#### *Material constants for the mixture*

The material constants of mixtures can be determined experimentally [22] or can be derived from the properties of the components. In the dimensionless analysis in this work, the set of input parameters consists of the porosity  $\hat{n}$ , Poisson's ratio of the skeleton  $\nu_s$ , the ratio of the bulk modulus of the fluid and the shear modulus of the skeleton  $K_f/\mu_s$ , and the ratio of the mass density of the fluid and that of the grains  $\rho_f/\rho_{gr}$  (both per unit volume of 'pure' material).

The elastic moduli of the mixture  $\mu$ ,  $\lambda$ ,  $R$ , and  $Q$  are computed using a simplification (for  $R$  and  $Q$ ) of the formulae proposed by Biot and Willis [22] based on the assumption that the compressibility of the mixture is much smaller than that of the solid skeleton and that of the fluid individually, and can be neglected (a common assumption in soil mechanics; [17])

$$\begin{aligned} \mu &= \mu_s \\ \lambda &= \lambda_s + Q^2/R \\ Q &= (1 - \hat{n})K_f \\ R &= \hat{n}K_f \end{aligned} \quad (11)$$

where

$$\lambda_s = \frac{2\nu_s}{1 - 2\nu_s} \mu_s = \text{Lamé constant for the skeleton} \quad (12)$$

For computation of the mass coefficients,  $\rho_{11}$ ,  $\rho_{22}$ , and  $\rho_{12}$ , the following relations proposed by Berryman [21] are used (as in [17])

$$\begin{aligned} \rho_{11} &= (1 - \hat{n})\rho_{gr} - \rho_{12} \\ \rho_{22} &= \hat{n}\rho_f - \rho_{12} \\ \rho_{12} &= -\hat{n}(\tau_\alpha - 1)\rho_f \end{aligned} \quad (13)$$

where

$$\tau_\alpha = 1 + \tau_r \frac{1 - \hat{n}}{\hat{n}} \geq 1 = \text{dynamic tortuosity} \quad (14)$$

Tortuosity is a dimensionless macroscopic parameter characterizing the resistance to flow of a fluid in a porous medium, in particular the effect that, on a microscopic scale, the paths of the fluid particles deviate from a straight line. It depends on the porosity,  $\hat{n}$ , as well as on the shape of the pores, through the parameter  $\tau_r$ . It has values  $1 \leq \tau_\alpha < \infty$ . As  $\hat{n} \rightarrow 1$  (pure fluid)  $\tau_\alpha \rightarrow 1$ , and as  $\hat{n} \rightarrow 0$  (pure solid)  $\tau_\alpha \rightarrow \infty$ . For pores formed by spherical grains, as assumed in this work,  $\tau_r = \frac{1}{2}$ , and

$$\tau_\alpha = \frac{1}{2} \left( 1 + \frac{1}{\hat{n}} \right) \quad (15)$$

It can be seen from Equation (11) that the dynamic mass coefficients represent physically mass densities, per unit volume of the mixture. If the coupling term  $\rho_{12}$  is neglected, then  $\rho_{11}$  and  $\rho_{22}$  represent the mass densities of the solid and fluid phases per unit volume of the mixture. Let  $\rho^{(s)}$ ,  $\rho^{(f)}$ , and  $\rho$  represent, respectively, the mass densities of the solid, fluid, and mixture, all per unit volume of the mixture. Then

$$\begin{aligned} \rho^{(s)} &= (1 - \hat{n})\rho_{gr} = \rho_{11} + \rho_{12} \\ \rho^{(f)} &= \hat{n}\rho_f = \rho_{22} + \rho_{12} \\ \rho &= \rho^{(s)} + \rho^{(f)} = \rho_{11} + \rho_{22} + 2\rho_{12} \end{aligned} \quad (16)$$

#### *Representation of the motion in the soil*

The motions of the soil skeleton,  $\mathbf{u}$ , and of the pore fluid,  $\mathbf{U}$ , can be represented as a sum of the free-field motion, indicated by superscript 'ff', which is the motion in the half-space without any excavations and structures, and a perturbation referred to as 'scattered waves', indicated by superscript 'R'

$$\begin{aligned} \mathbf{u} &= \mathbf{u}^{ff} + \mathbf{u}^R \\ \mathbf{U} &= \mathbf{U}^{ff} + \mathbf{U}^R \end{aligned} \quad (17)$$

As mentioned earlier, the motion of the fluid can be expressed as a function of the motion in the solid, which remains to be the only unknown. Hence, from now on, only the potentials in the soil are mentioned explicitly in the further development of the solution of the soil-structure interaction problem.

In this article, the scattered waves (in the solid) are represented by a triplet of potentials,  $\phi_1^R$ ,  $\phi_2^R$ , and  $\psi^R$  (respectively, for the fast P-wave, slow P-wave, and S-wave), each expanded in Fourier–Bessel series with period  $2\pi$ , representing outgoing cylindrical waves with the origin at point  $O_1$  (see Figure 2 showing an excavation in the soil where the foundation is embedded):

$$\begin{aligned}\phi_1^R &= \sum_{n=0}^{\infty} (A_{1,n} \cos n\theta_1 + B_{1,n} \sin n\theta_1) H_n^{(1)}(k_{P1}r_1) e^{-i\omega t} \\ \phi_2^R &= \sum_{n=0}^{\infty} (E_{1,n} \cos n\theta_1 + F_{1,n} \sin n\theta_1) H_n^{(1)}(k_{P2}r_1) e^{-i\omega t} \\ \psi^R &= \sum_{n=0}^{\infty} (C_{1,n} \sin n\theta_1 + D_{1,n} \cos n\theta_1) H_n^{(1)}(k_S r_1) e^{-i\omega t}\end{aligned}\quad (18)$$

Then the radial and tangential components of the displacements and stresses in the skeleton due to the scattered waves can be computed by substitution of the representations in Equations (18) in Equations (7) and (5). The resulting lengthy expressions can be found in [8]. The displacements and stresses of the free-field motion, usually specified in rectangular coordinates, can also be expanded in Fourier–Bessel series of the same form as those for the scattered waves, but only if it consists of plane waves, as such series diverge for surface waves. Instead, for surface waves, the displacements and stresses along the contact between the foundation and the soil, which is a cylindrical surface with constant radius, are expanded in finite Fourier series for the purpose of applying the boundary conditions on that surface, as discussed in the following section.

#### *Compatibility of displacements on the contact surface*

The harmonic excitation, the motion of the rigid foundation can be expressed as

$$\begin{Bmatrix} V \\ \Delta \\ \varphi a \end{Bmatrix} = \begin{Bmatrix} V_0 \\ \Delta_0 \\ \varphi_0 a \end{Bmatrix} e^{-i\omega t}\quad (19)$$

Along the contact surface  $\Sigma : r_1 = b, -\theta_0 \leq \theta \leq \theta_0, \theta_0 = \sin^{-1}(a/b)$  (Figure 2), the displacements of the skeleton are constrained by the displacements of the foundation, and the motion of the fluid is constrained by the drainage condition. Perfect bond between the skeleton and the foundation, and perfectly sealed contact (undrained boundary) preventing flow of fluid through this boundary imply

$$\begin{Bmatrix} u_{r_1} \\ u_{\theta_1} \\ (u_{r_1} - U_{r_1}) \end{Bmatrix}_{\Sigma}^{\text{ff}} + \begin{Bmatrix} u_{r_1} \\ u_{\theta_1} \\ (u_{r_1} - U_{r_1}) \end{Bmatrix}_{\Sigma}^R = \begin{bmatrix} \cos \theta_1 & \sin \theta_1 & (d/a) \sin \theta_1 \\ -\sin \theta_1 & \cos \theta_1 & -b/a + (d/a) \cos \theta_1 \\ 0 & 0 & 0 \end{bmatrix} \begin{Bmatrix} V_0 \\ \Delta_0 \\ \varphi_0 a \end{Bmatrix} e^{-i\omega t}\quad (20a)$$

Similarly, perfect bond between the skeleton and the foundation, and unsealed contact (drained boundary) permitting free flow of the pore fluid through this boundary imply

$$\begin{Bmatrix} u_{r_1} \\ u_{\theta_1} \\ s \end{Bmatrix}_{\Sigma}^{\text{ff}} + \begin{Bmatrix} u_{r_1} \\ u_{\theta_1} \\ s \end{Bmatrix}_{\Sigma}^{\text{R}} = \begin{bmatrix} \cos \theta_1 & \sin \theta_1 & (d/a) \sin \theta_1 \\ -\sin \theta_1 & \cos \theta_1 & -b/a + (d/a) \cos \theta_1 \\ 0 & 0 & 0 \end{bmatrix} \begin{Bmatrix} V_0 \\ \Delta_0 \\ \varphi_0 a \end{Bmatrix} e^{-i\omega t} \quad (20b)$$

Equations (20a) and (20b) describe the compatibility conditions for the motion of the foundation and that of the soil, and the matrix on the right-hand side of each equation is called the foundation influence matrix.

The condition on the stresses in the soil is that they should be such that the foundation is in dynamic equilibrium under the action of all forces. The application of this condition requires integration of the stresses in the soil along the contact surface, presented in the following section.

#### *Internal stress in the soil and external forces on the contact surface*

Next we compute vertical and horizontal forces  $f_z^{(s)}$  and  $f_x^{(s)}$ , and moment about  $O$ ,  $M_0^{(s)}$ , which act on the soil producing the overall stress field in the soil, shown in Figure 2. We also introduce a generalized force vector notation for this triplet of forces and moment  $\mathbf{F} = \{f_z, f_x, M_0/a\}^T$  and refer to it as *the force*, and generalized displacement vector  $\Delta = \{V, \Delta, \varphi a\}^T$ , which we refer to it as *the displacement*. Further, for harmonic motion,  $\Delta = \Delta_0 e^{-i\omega t}$ , where  $\Delta_0$  is its complex amplitude.

Following the representation in Equation (17), the resultant force vector,  $\mathbf{F}^{(s)}$ , is the sum

$$\begin{aligned} \mathbf{F}^{(s)} &= \mathbf{F}_{\text{ff}}^{(s)} + \mathbf{F}_{\text{R}}^{(s)} \\ &= \int_{-\theta_0}^{\theta_0} b \begin{bmatrix} -\cos \theta_1 & +\sin \theta_1 \\ -\sin \theta_1 & -\cos \theta_1 \\ -(d/a) \sin \theta_1 & b/a - (d/a) \cos \theta_1 \end{bmatrix} \left\{ \begin{Bmatrix} \tau_{r_1 r_1} + s \\ \tau_{r_1 \theta_1} \end{Bmatrix}_{\Sigma}^{\text{ff}} + \begin{Bmatrix} \tau_{r_1 r_1} + s \\ \tau_{r_1 \theta_1} \end{Bmatrix}_{\Sigma}^{\text{R}} \right\} d\theta_1 \end{aligned} \quad (21)$$

where  $\mathbf{F}_{\text{ff}}^{(s)}$  is integral of the stresses due to the free-field motion, and  $\mathbf{F}_{\text{R}}^{(s)}$  is an integral of the stresses due to the so-called ‘scattered’ waves, which represent the difference between the actual wave field and the free-field motion. Further, the compatibility of displacements (Equations (20)) implies that  $\mathbf{F}_{\text{R}}^{(s)}$  can be split into two parts:

$$\mathbf{F}_{\text{R}}^{(s)} = \mathbf{F}_{\text{scat}}^{(s)} + \mathbf{F}_{\Delta}^{(s)} \quad (22)$$

where  $\mathbf{F}_{\text{scat}}^{(s)}$  is some function of the *displacements* along the contact surface due to the free-field motion (known), and  $\mathbf{F}_{\Delta}^{(s)}$  is a function of the motion of the foundation  $\Delta$  (unknown). The latter can be expressed as

$$\mathbf{F}_{\Delta}^{(s)} = 2\mu[K^{(s)}]\Delta \quad (23)$$

where the  $3 \times 3$  matrix  $[K^{(s)}]$  is the dimensionless complex stiffness matrix of the foundation. Its real part represents the foundation stiffness, and its imaginary part the damping due to radiation of energy in the semi-infinite soil medium.

The expressions for  $[K^{(s)}]$  and for  $\mathbf{F}_{\text{scat}}^{(s)}$  for both drained and undrained boundary can be found in [8]. Finally, Equations (22) and (23) imply that the resultant force can be split into three parts:

$$\mathbf{F}^{(s)} = \mathbf{F}_{\text{ff}}^{(s)} + \mathbf{F}_{\text{scat}}^{(s)} + \mathbf{F}_{\Delta}^{(s)} \quad (24)$$

where the first two parts depend only on the wave excitation and shape of the contact surface, whereas  $\mathbf{F}_{\Delta}^{(s)}$  depends only on the displacement of the foundation. Equation (24) implies that, when there is no incident wave motion,  $\mathbf{F}^{(s)} = \mathbf{F}_{\Delta}^{(s)}$ , which means that  $\mathbf{F}_{\Delta}^{(s)}$  is counteracted by stresses in the soil generated by its deformation due to vibration of the foundation,  $\Delta$ , in the absence of incident wave motion. Equivalently, if the foundation is at rest under the action of the incident wave motion, then  $\mathbf{F}^{(s)} = \mathbf{F}_{\text{ff}}^{(s)} + \mathbf{F}_{\text{scat}}^{(s)}$  is the force required to keep it at rest, under the action of stresses generated by the free-field motion and by waves scattered from the excavation. Then force  $\mathbf{F}_{\text{driv}}^{(s)}$  can be introduced, which is the sum

$$\mathbf{F}_{\text{driv}}^{(s)} = \mathbf{F}_{\text{ff}}^{(s)} + \mathbf{F}_{\text{scat}}^{(s)} \quad (25)$$

referred to as the foundation driving force, representing the effective driving force, which is integral of the stresses of the free-field motion (along the excavation) modified by the scattered waves from the excavation. This modification of the wave excitation due to pure scattering, in the absence of any external forces, is referred to as kinematic interaction, whereas the modification due to feedback forces between the structure and the soil is referred to as dynamic interaction. Finally

$$\mathbf{F}^{(s)} = \mathbf{F}_{\text{driv}}^{(s)} + \mathbf{F}_{\Delta}^{(s)} \quad (26)$$

#### *Dynamic equilibrium of the foundation*

The only remaining unknown is the foundation displacement vector,  $\Delta$ , which can be determined from the dynamic equilibrium of the foundation. Figure 3 shows a free-body diagram of the foundation, which is subjected to the forces from the building,  $\mathbf{F}^{(b)}$ , and the forces from the soil,

$$\mathbf{F}^{(s)} = \mathbf{F}_{\text{driv}}^{(s)} + 2\mu[K^{(s)}]\Delta \quad (27)$$

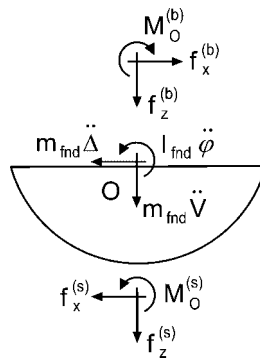


Figure 3. Dynamic equilibrium of the foundation.

For small amplitudes of the response, the forces from the building can be represented in terms of the displacement vector,  $\Delta$ , as follows [20]:

$$\mathbf{F}^{(b)} = m_b \omega^2 [M_b] \Delta \quad (28)$$

where  $[M_b]$  is a dimensionless matrix that depends on the building model and characteristics,  $m_b$  is the mass per unit length (in the  $y$ -direction) of the shear beam. The dynamic equilibrium of forces acting on the foundation implies

$$\omega^2 m_{\text{fnd}} [M_{\text{fnd}}] \Delta - \mathbf{F}_{\text{driv}}^{(s)} - 2\mu [K^{(s)}] \Delta + \omega^2 m_b [M_b] \Delta = \mathbf{0} \quad (29)$$

where  $m_{\text{fnd}}$  is the mass per unit length (in the  $y$ -direction) of the foundation,  $[M_{\text{fnd}}]$  is the foundation dimensionless mass matrix. Expressions for  $[M_b]$  and  $[M_{\text{fnd}}]$  can be found in [16,20].

Finally, one can solve for  $\Delta$  by inverting a  $3 \times 3$  matrix

$$\Delta = \left[ \frac{\omega^2 m_{\text{fnd}}}{2\mu} [M_{\text{fnd}}] + \frac{\omega^2 m_b}{2\mu} [M_b] - [K^{(s)}] \right]^{-1} 2\mu \mathbf{F}_{\text{driv}}^{(s)} \quad (30)$$

## RESULTS AND ANALYSIS

The numerical results were computed using a FORTRAN computer program. For viscous fluids and finitely permeable skeleton, the wave velocities in the half-space are complex valued, which requires computation of Bessel functions of complex arguments. For this purpose, subroutines from Zhang and Jin [23] were used. The computer program was written in terms of dimensionless parameters, defined using as reference: length  $a$ , material modulus  $\mu_s$ , and mass density  $\rho_{\text{gr}}$ . Then, the system response is a function of the following dimensionless parameters: stiffness of the fluid relative to the skeleton, defined through the ratio  $K_f/\mu_s$  and Poisson's ratio  $\nu_s$ ; mass density of the skeleton relative to the fluid, defined through the ratio  $\rho_{\text{gr}}/\rho_f$  and the porosity  $\hat{n}$ ; mass of the building relative to the mass of the foundation, and mass of the foundation relative to the mass of the replaced soil, through the ratios  $m_b/m_{\text{fnd}}$  and  $m_{\text{fnd}}/m_{\text{gr}}$ , where,  $m_{\text{gr}} = A_{\text{fnd}}\rho_{\text{gr}}$  is the mass of the excavated soil (per unit length) if there were no voids, and  $A_{\text{fnd}}$  is the area of the foundation; the flexibility of the building relative to that of the soil, through the ratio  $\epsilon = (V_{\text{ref}}H)/(V_{S,b}a) = [(\omega H)/V_{S,b}]/[(\omega a)/V_{\text{ref}}]$  = ratio of the number of wavelength in the shear beam in length  $H$  and the number of reference wavelengths in the soil in length  $a$ ; dimensionless frequency  $\eta = \omega a/(\pi V_{\text{ref}})$ , where  $V_{\text{ref}} = \sqrt{\mu_s/\rho_{\text{gr}}}$  is a reference velocity; foundation shape, through the ratio  $h/a$ ; and on the type, amplitude, and angle of the incident waves.

### *Input model parameters*

The input parameters corresponding approximately to the NS response of Millikan library are as chosen in [9] based on information provided in [11] (building weight =  $1.05 \times 10^8$  N, foundation weight =  $0.14 \times 10^8$  N, building height = 44 m, foundation depth = 4 m, and building in plan dimensions = 21 m  $\times$  23 m). The assumed *fixed-base* frequency is  $f_1 = 2.5$  Hz, which results in values of the system frequency predicted by the model similar as the observed values. The reference length is  $a = 12$  m, and  $b/a = 1$  (semi-circular foundation). The mass ratios for the model are  $m_b/m_f = 7.5$  and  $m_f/m_{\text{gr}} = 0.1$  (based on the soil mass discussed below).

Table I. Wave velocities for dry, undrained, and fully saturated soil with no seepage force.

Condition	$K_f/\mu_s$	$\rho_f/\rho_{gr}$	Poisson ratio	$V_S$	$V_{P1}$	$V_{P2}$
Dry	0.0001	0.001	0.30	300	561	55
Saturated	15.0890	0.371	0.30	285	1805	331
Undrained	0.0001	0.371	0.48	285	1457	3

The soil porosity is  $\hat{n} = 0.4$ , Poisson's ratio of the skeleton is  $\nu_s = 0.3$ , the mass density of the grain is  $\rho_{gr} = 2.7 \times 10^3 \text{ kg/m}^3$ , and  $\mu_s$  is taken so that it results in shear wave velocity of dry soil  $V_{S,dry} = \sqrt{\mu_s/[(1 - \hat{n})\rho_{gr}]} = 300 \text{ m/s}$ . The pore fluid is water with mass density  $\rho_f = 10^3 \text{ kg/m}^3$  and bulk modulus  $K_f = 2.2 \times 10^9 \text{ Pa}$  (which gives a bulk wave velocity of 1483 m/s). These parameters imply  $K_f/\mu_s = 15.089$ . For dry soil, values  $\rho_f/\rho_{gr} = 0.001$ ,  $K_f/\mu_s = 0.0001$ , and Poisson ratio is  $\nu_s = 0.3$  were assigned, whereas for undrained soil, values  $\rho_f = 10^3 \text{ kg/m}^3$ ,  $K_f/\mu_s = 0.0001$ , and Poisson ratio  $\nu_s = 0.48$  are assigned. This leads to wave velocities for the dry solid, undrained solid, and velocities of the saturated poroelastic soil with no seepage force (all frequency independent) listed in Table I.

The choice of values for the finite skeleton permeability and fluid viscosity (ignored in [9]) was made as follows. The dissipation depends on the ratio  $\hat{\mu}/\hat{k}$ , where  $\hat{\mu}$  is the absolute viscosity of the fluid, and  $\hat{k}$  is the intrinsic permeability of the skeleton. The absolute viscosity of water at about 25°C is  $\hat{\mu}_w = 0.89 \times 10^{-3} \text{ Pa} \cdot \text{s}$  (1 Pa · s = 1 N s/m<sup>2</sup>). In this work, a rounded value  $\hat{\mu} = \hat{\mu}_w = 10^{-3} \text{ N s/m}^2$  is used. The intrinsic permeability of the skeleton depends on the type of geologic material. Pervious consolidated geo materials, such as highly fractured rock, and pervious unconsolidated geo materials such as well-sorted gravel and well-sorted sand and gravel, have intrinsic permeability  $\hat{k}$  in the range  $10^{-6} - 10^{-10} \text{ m}^2$ . Semi-pervious consolidated geo materials, such as oil reservoir rocks and fresh sandstone, and semi-pervious unconsolidated geo materials, such as very fine sand, silt, loess, and loam, have  $\hat{k}$  in the range  $10^{-11} - 10^{-14} \text{ m}^2$  [24]. Geo materials with  $\hat{k}$  in the range  $10^{-15} - 10^{-19} \text{ m}^2$  are considered to be impervious. In this article, results are shown for  $10^{-10} \leq \hat{k} < \infty$ , where  $\hat{k} \rightarrow \infty$  corresponds to the case when the effects of the seepage force are neglected.

The upper bound of frequency for which Biot's theory [7] is valid is constrained by the requirements that (1) the flow of the fluid in the pores is laminar and (2) the wavelengths are much larger than the size of the pores. The first requirement implies frequency bound  $f_t = (\pi\hat{\nu})/(4d^2)$ , where  $d$  is the diameter of the pores and  $\hat{\nu}$  is the kinematic viscosity, which is related to the dynamic viscosity  $\hat{\mu}$  and fluid density  $\rho_f$  by  $\hat{\nu} = \hat{\mu}/\rho_f$  [7]. This implies maximum frequencies  $f_t = 10\,000 \text{ Hz}$  for  $d = 0.01 \text{ mm}$  (silt),  $f_t = 100 \text{ Hz}$  for  $d = 0.1 \text{ mm}$  (sands), and  $f_t = 10 \text{ Hz}$  for  $d = 1 \text{ mm}$  (coarse sands to gravel). The soil underneath the foundation of Millikan library has been described as alluvium consisting of medium to dense sands mixed with gravels [3,5] for which the maximum frequency considered in this work of 25 Hz appears to be appropriate.

### Results for foundation complex stiffness

Figure 4 shows results for the foundation complex stiffness matrix for dry soil, undrained soil, and fully saturated soil for several values of intrinsic skeleton permeability. For drained (open) contact surface, results are shown for intrinsic skeleton permeability  $\hat{k} \equiv K \geq 10^{-7}$ ,  $10^{-8}$ , and

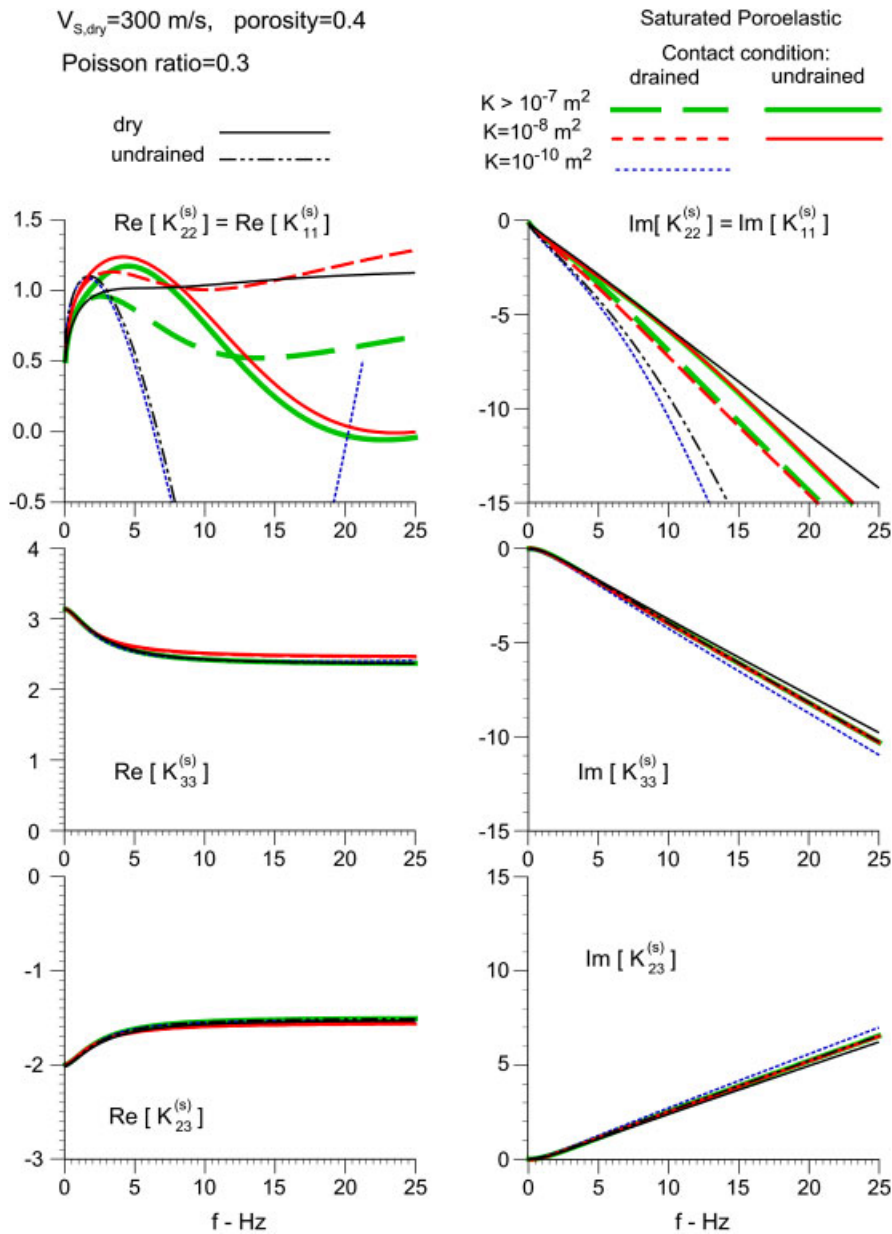


Figure 4. Foundation complex stiffness matrix coefficients for model parameters corresponding approximately to Millikan library NS response. Left, real part; Right, imaginary part.

$10^{-10}$  m<sup>2</sup>. For undrained (sealed) contact surface, results are shown for  $\hat{k} \equiv K \geq 10^{-7}$  and  $10^{-8}$  m<sup>2</sup>. It is noted that the results for high but finite permeability ( $\hat{k} \equiv K \geq 10^{-7}$  m<sup>2</sup>) are indistinguishable from those for infinite permeability. The plots on the left-hand side show the real parts and those on the right-hand side show the imaginary parts of the terms of the complex

stiffness matrix. The terms  $K_{11}^{(s)}$ ,  $K_{22}^{(s)}$ , and  $K_{33}^{(s)}$  represent, respectively, the vertical, horizontal, and rocking stiffness, and  $K_{23}^{(s)} = K_{32}^{(s)}$  represents the coupling term. For semi-circular foundation and under the simplifying assumption of this model, the horizontal and vertical stiffness coefficients have same values.

Comparison of the results for the different stiffness coefficients shows that the horizontal and vertical stiffness coefficients for this model are most affected by the presence of pore water. The small effect on the rocking stiffness and coupling term is due to the specific shape of the foundation (semi-cylindrical) in relation to the particular degree of freedom, and this conclusion cannot be generalized to foundations of different shapes. The small effect of the pore water on the rocking stiffness can be explained by the fact that rocking driving motion excites the adjacent soil to move tangentially to the (2D cylindrical) contact surface, whereas the effect of the pore water becomes significant if there is a significant component of this motion perpendicular to the contact surface, over a significant area. Similar effects observed by other authors for different foundation shapes are the small effect on the horizontal stiffness for surface foundations and the small effect on the torsional stiffness for circular disk foundations. From now on, only the effects of different conditions on the horizontal/vertical stiffness will be discussed.

Comparison of the results for the horizontal/vertical stiffness for saturated soil with very high skeleton permeability ( $\hat{k} \equiv K \geq 10^{-7} \text{ m}^2$ ) shows that the stiffness (real part) is larger for undrained (sealed) contact, whereas the damping (imaginary part) is larger for undrained (open) contact. For the values of permeability considered here, the foundation stiffness increases when the soil permeability decreases (i.e. when the damping in the soil due to the seepage force increases). The foundation damping is affected a little if the contact is undrained, whereas it increases significantly if the contact is drained. Hence, from the point of view of radiation damping, drained soil–foundation boundary is more beneficial than an undrained one. The results also show that, in the case of a drained contact, for small soil permeability the foundation stiffness and damping are close to those for undrained soil. Finally, for small frequencies (below about 4 Hz), which is where the fundamental fixed-base frequency of the building falls, the foundation stiffness for saturated soil, for all the cases shown, is larger than for dry soil, which is expected to produce an increase in the first system frequency as a result of the water saturation.

#### *Results for the system response*

Figure 5 shows results for the system response to horizontal driving motion with unit amplitude. Hence, in these results only the effects of the dynamic soil structure interaction are considered. It is noted that ignoring the effects of the kinematic interaction, for rigid foundations, overestimates the effective input motion at higher frequencies. The top, middle, and bottom plots in Figure 5 show results for the magnitudes of the relative horizontal building response, the absolute foundation horizontal displacement (of point O), and the rotation of the foundation (normalized to displacement units by multiplication by the characteristic length  $a$ ). The different curves correspond to the same parameters and conditions as in Figure 4. It can be seen that the system response for saturated poroelastic soil has the same general features as for elastic soil.

Figure 6 shows an enlarged view of the building's relative response near the first system frequency, which is of primary interest in this paper. It can be seen that, for highly permeable

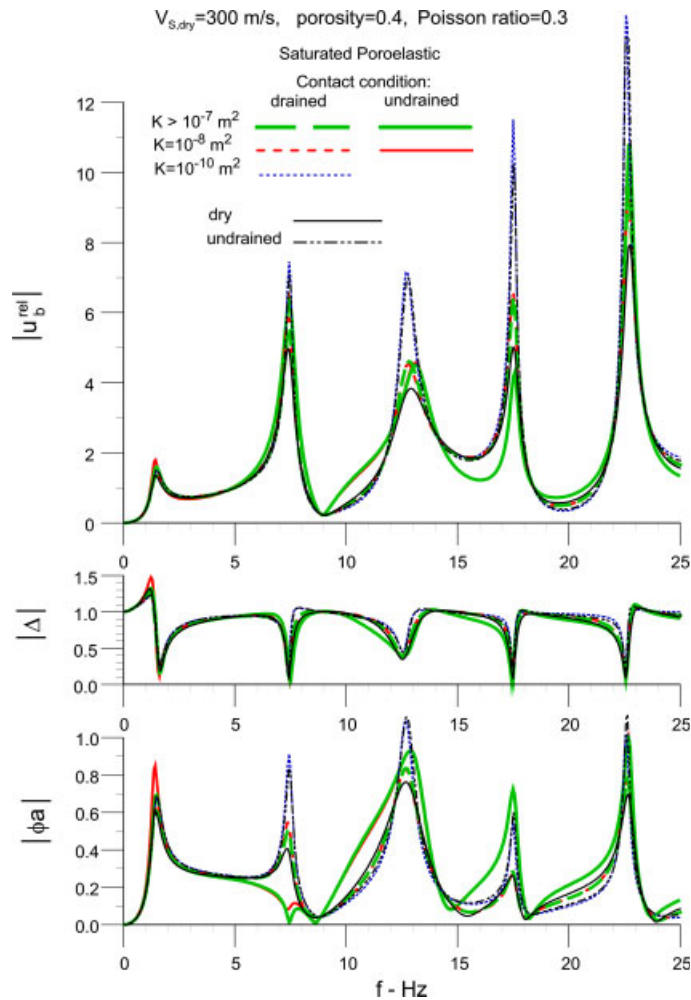


Figure 5. System response for model parameters corresponding approximately to Millikan library NS response.

soil ( $\hat{k} \equiv K \geq 10^{-7}$  m<sup>2</sup>), the increase in the frequency of this peak is larger for undrained (sealed) contact than for drained (open) contact. However, for less permeable soil, the increase in frequency is larger for the drained boundary, and approaches that for undrained soil, for which the increase is 0.06 Hz (from 1.44 to 1.5 Hz) or 4%. It is noted that for undrained (sealed) contact, the trend may reverse for low soil permeability.

## DISCUSSION AND CONCLUSIONS

A simple 2D soil–structure interaction model in a two-phase soil medium is presented, which can be used to gain understanding of the nature and degree of changes in the measured

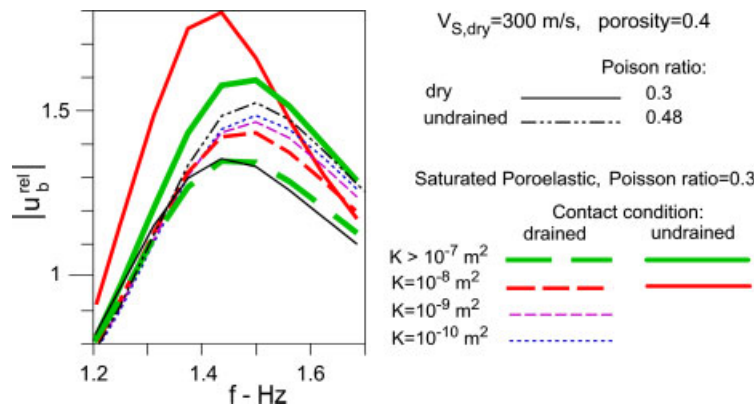


Figure 6. Enlarged view of the first peak in the building's relative roof response of the model corresponding to Millikan library.

(apparent) frequencies of structures due to water saturation of the soil. In this model, the building is represented by a shear wall supported by a semi-cylindrical rigid foundation embedded in a poroelastic half-space, and the motion in the soil is modeled using Biot's theory of wave propagation in fluid-saturated porous media [7]. Although the main limitation of Biot's theory [7] is its linearity, it is appropriate for the problem in this paper, which involves interpretation of small amplitude response of soils and structures to ambient excitation. Results were shown for the foundation complex stiffness matrix and for the system response to horizontal driving force for model parameters that correspond approximately to the NS response of Millikan library, and the analysis focused on the effect of the soil permeability, which is finite in this model. The results show that, for small soil permeability and for drained (open) contact between the foundation and the soil, the results for poroelastic soil approach those for undrained soil, for which the *increase* in the first system frequency predicted by this model is the largest (about 4%). The predicted effect is similar for undrained (sealed) contact when the permeability of the skeleton is large. The results show that, for small excitation and for medium soft soils with shear wave velocity near the surface of about 300 m/s, the effect of the pore water on the apparent frequency of buildings such as Millikan library is generally small (of the order of few percent), and the trend is an increase. The trend and degree of the predicted change agree with the observations at Millikan library. Hence, poroelasticity and *changes in the soil* surrounding the foundation due to the presence of pore water can explain the observed shift in the first apparent frequency of the NS response of this building. The analysis, however, does not exclude other possible causes for the observed effects. In addition, the analysis in this paper does not attempt to predict or explain a shift in the system frequency due to changes in the *height of the water table* underneath the site [4]. The computed variations of the foundation stiffness with frequency (see Figure 4, top-left) show that the foundation stiffness for saturated soil can be smaller than that for dry soil for larger frequencies, suggesting a decrease in frequency for the higher modes during heavy rainfall (which agrees with the observations at Millikan library [3]). This also suggests that the trend (sign and amount of the shift) observed at Millikan library cannot be generalized to all structures and soils. The significance and nature of the effect of saturation of the soil will depend on the values of the *dimensionless* parameters of

the model controlling the response, as stated in this paper, such as stiffness of the soil relative to the building and the dimensions of the building and foundation as combined in parameter  $\epsilon$ , the ratio of rigidities of the pore fluid (water in this case) and soil skeleton ( $K_f/\mu_s$ ), mass of the building relative to the mass of replaced soil by the foundation, and dimensionless frequency  $\eta = \omega a/(\pi V_{\text{dry}})$ . An insight into the interplay of these parameters in their influence on the final effect can be obtained by a detailed parametric study, to be presented in other publications. Finally, the model also predicts larger *radiation* damping when the soil is saturated, which increases with decreasing soil permeability. A detailed study of the effect of saturation of the apparent damping is also out of the scope of this study.

#### ACKNOWLEDGEMENTS

The authors are grateful to an anonymous reviewer for his detailed comment, which improved the clarity of this paper.

#### REFERENCES

1. Chang PC, Flatau A, Liu SC. Review paper: health monitoring of civil infrastructure. *Structural Health Monitoring* 2003; **2**(3):257–267.
2. Doebling SW, Farrar CR, Prime MB, Shevitz DW. Damage identification and health monitoring of structural and mechanical systems from changes in their vibration characteristics: a literature review. *Report LA-13070-MS*, Los Alamos National Laboratory, Los Alamos, NM, 1996.
3. Clinton JF, Bradford SK, Heaton TH, Favela J. The observed wander of the natural frequencies in a structure. *Bulletin of the Seismological Society of America* 2006; **96**(1):237–257.
4. Asghari A, Johnson EA, Nigbor RL. Environmental effects on identified parameters of the NEES SFSI test structure. *Proceedings of the 4th World Conference on Structural Control and Monitoring*, 11–13 July 2006, San Diego, CA, Paper: 4WCSCM-331, 2006.
5. Luco J, Trifunac MD, Wong HL. On the apparent change in dynamic behavior of a 9-story reinforced-concrete building. *Bulletin of the Seismological Society of America* 1987; **77**(6):1961–1983.
6. Udawadia FE, Trifunac MD. Time and amplitude dependent response of structures. *Earthquake Engineering and Structural Dynamics* 1974; **2**(4):359–378.
7. Biot MA. Theory of propagation of elastic waves in a fluid-saturated porous solid: I low-frequency range. *Journal of Acoustical Society of America* 1956; **28**(2):168–178.
8. Todorovska MI, Al Rjoub Y. Effects of rainfall on soil–structure system frequency: examples based on poroelasticity and a comparison with full-scale measurements. *Soil Dynamics and Earthquake Engineering* 2006; **26**(6–7):708–717.
9. Todorovska MI, Al Rjoub Y. Plain strain soil–structure interaction model for a building supported by a circular foundation embedded in a poroelastic half-space. *Soil Dynamics and Earthquake Engineering* 2006; **26**(6–7):694–707.
10. Foutch DA, Luco JE, Trifunac MD, Udawadia FE. Full scale three-dimensional tests of structural deformations during forced excitation of a nine-story reinforced concrete building. *Proceedings of the US National Conference on Earthquake Engineering*, Ann Arbor, MI, 1975; 206–215.
11. Luco JE, Wong HL, Trifunac MD. Soil–structure interaction effects on forced vibration tests. *Technical Report 86-05*, Department of Civil Engineering, University of Southern California, Los Angeles, CA, 1986.
12. Halpern MR, Christiano P. Steady-state harmonic response of a rigid plate bearing on a liquid-saturated poroelastic half space. *Earthquake Engineering and Structural Dynamics* 1986; **14**:439–454.
13. Bougacha S, Roesset JM, Tassoulas JL. Dynamic stiffness of foundations on fluid filled poroelastic stratum. *Journal of Engineering Mechanics—ASCE* 1993; **119**(8):1649–1662.
14. Bougacha S, Tassoulas JL, Roesset JM. Analysis of foundations on fluid-filled poroelastic stratum. *Journal of Engineering Mechanics—ASCE* 1993; **119**(8):1632–1648.
15. Japon BR, Gallego R, Dominguez J. Dynamic stiffness of foundations on saturated poroelastic soils. *Journal of Engineering Mechanics—ASCE* 1997; **123**(11):1121–1129.
16. Todorovska MI. Effects of the wave passage and the embedment depth during building–soil interaction. *Soil Dynamics and Earthquake Engineering* 1993; **12**(6):343–355.

17. Lin CH, Lee VW, Trifunac MD. The reflection of plane waves in a poroelastic half-space saturated with inviscid fluid. *Soil Dynamics and Earthquake Engineering* 2005; **25**:205–223.
18. Luco JE. Dynamic interaction of a shear wall with the soil. *Journal of Engineering Mechanics—ASCE* 1969; **95**:333–346.
19. Trifunac MD. Interaction of a shear wall with the soil for incident plane SH-waves. *Bulletin of the Seismological Society of America* 1972; **2**:63–83.
20. Todorovska MI. In-plane foundation–oil interaction for embedded circular foundations. *Soil Dynamics and Earthquake Engineering* 1993; **12**(5):283–297.
21. Berryman JG. Confirmation of Biot's theory. *Applied Physics Letters* 1980; **34**(4):382–384.
22. Biot MA, Willis DG. The elastic coefficients of a theory of consolidation. *Journal of Applied Mechanics, ASME* 1957; **29**:594–601.
23. Zhang S, Jin J. *Computation of Special Functions*. Wiley: New York, 1996.
24. Bear J. *Dynamics of Fluids in Porous Media*. American Elsevier Publ. Co.: New York, 1972.